THE JOURNAL OF PHYSICAL CHEMISTRY A
A JOURNAL OF THE AMERICAN CHEMICAL SOCIETY

pubs.acs.org/JPCA

Article

Multiconfiguration Pair-Density Functional Theory for Vertical Excitation Energies in Actinide Molecules

Arup Sarkar and Laura Gagliardi*

Cite This: *J. Phys. Chem. A* 2023, 127, 9389−9397

Read Online

ACCESS | Metrics & More | Article Recommendations | Supporting Information

ABSTRACT: Modeling actinides with electronic structure theories is challenging because these systems present a strong ligand field and metal−ligand covalency. We systematically investigate the effectiveness of pair-density functional theory (PDFT) for the calculation of vertical excitation energies in An(III), $[An^{III}Cl_6]^{3-}$, and $[An^{VI}O_2]^{2+}$ (An = U, Np, Pu, and Am). We compare the performance of PDFT, hybrid PDFT, and multistate PDFT with traditional active-space methods followed by perturbation theory, like multistate CASPT2, and with experimental data. Overall, multistate PDFT gives quantitative agreement with multistate CASPT2 at a significantly reduced computational cost.

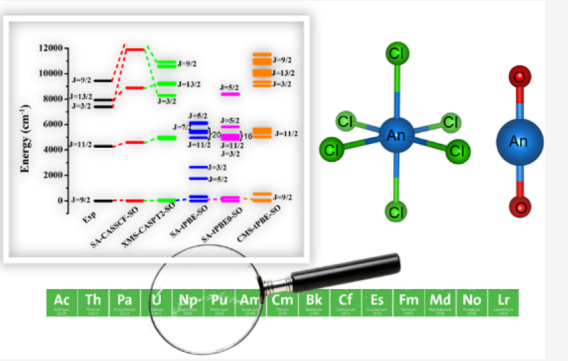

1. INTRODUCTION

Actinides are present in nuclear and radioactive processes; therefore, understanding their electronic structure is very important.[1,2] Being able to accurately describe the behavior of f-electrons in computations, including strong correlation effects, spin−orbit coupling, and multiplet complexity, is a challenge. This is especially true because actinides possess a strong crystal field and spin−orbit coupling (SOC).[3−7] A multiconfiguration treatment, including SOC, is indispensable for calculations on actinides. Active-space self-consistent field calculations account for static correlation (near degeneracy effect) and are usually followed by a perturbative (second-order) treatment that recovers dynamic correlation, which is very important for actinide molecules to correctly describe metal−ligand covalency[8,9] because the 5f valence orbitals in actinides are diffused and hence exert a strong ligand field.[10−13] However, multireference second-order perturbation theory (MRPT2) methods are very expensive when the active space is large (e.g., beyond the 5f shell) and also when many electronic states are computed, using state average procedures.[7,11,14]

Multiconfigurational pair-density functional theory (MC-PDFT) combines a MCSCF wave function with a generalization of DFT and can efficiently treat strongly correlated systems at a significantly reduced cost compared to MRPT2 methods.[15,16] By using complete active space (CAS),[15] restricted active space (RAS),[17] generalized active space (GAS),[18] localized active space (LAS),[19] and density matrix renormalization group (DMRG)[20,21] wave functions, multimetallic systems, magnetic exchange coupling, potential energy surfaces, and nonadiabatic couplings have been accurately described.[22] MC-PDFT has also been employed to perform geometry optimizations and compute bond dissociation energies of actinide systems.[23] Hu et al. used DMRG-PDFT with large active spaces such as (34e, 44o) and (38e, 40o) to understand the electronic structure and bonding features of various oxo-bridged dimeric actinide molecules.[24] However, to describe the correct topology of potential energy surfaces at conical interactions, which are important for spectroscopy and photochemistry, one needs to consider multistate PDFT (MS-PDFT) similar to the MS-CASPT2[25] and QD-NEVPT2[26] methods. The recently developed compressed-state multistate PDFT (CMS-PDFT) method[27] has been shown to outperform other multistate PDFT methods[28] in obtaining smooth potential energy surfaces, conical interactions, and accurate dipole moment calculations both for ground and excited states.[27,29,30]

Relativistic effects in strongly correlated lanthanide- and actinide-based molecules can be treated in several ways. Both scalar relativistic effects and SOC can be described simultaneously using variational exact two-component X2C-MCSCF, X2C-MRPT2, and X2C-MC-PDFT frameworks.[31−34] However, fully variational relativistic methods are very expensive and have yet to be tested with reasonable size molecules. On the other hand, quasi-degenerate perturbative SO coupling schemes with state interaction obtained from the

Received: August 29, 2023
Revised: October 14, 2023
Accepted: October 15, 2023
Published: October 27, 2023

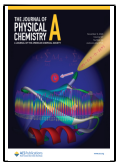

MCSCF or MS-PDFT states are well established and can be employed for large systems.[35−37]

Vertical excitation energies in transition metal complexes have previously been computed using the CMS-PDFT method, showing promising results for future applications of this method.[35] Compared to transition metal complexes, SOC or zero-field splitting (ZFS) is more prominent in actinide-based systems, making them potential candidates for single-molecule magnet applications.[6,11,14,38,39] It is thus important to benchmark PDFT methods for predicting the electronic excited states of actinides.

Toward this goal, we use MC-PDFT, hybrid MC-PDFT (HMC-PDFT), and CMS-PDFT to compute the electronic excitations of the An(III), $[An^{III}Cl_6]^{3-}$, $[An^{VI}O_2]^{2+}$ (An = U, Np, Pu, and Am) species and compare their performance with other multireference methods and available experimental data. This paper is organized as follows: in Section 2, we describe the computational methods; in Section 3, we present the benchmarking results of vertical excitation energies for the various actinide species. Finally, in Section 4, we offer some conclusions.

2. COMPUTATIONAL METHODOLOGY

All the calculations were performed using *OpenMolcas* v. 22.10.[40] For all of the systems, D_{2h} symmetry was imposed throughout the calculations. The geometries of the $[An^{III}Cl_6]^{3-}$ anions, optimized using state average-CASSCF-NEVPT2-SO, were taken from ref 5. The geometries of the $[AnO_2]^{2+}$ cations, optimized using SO-CASPT2, were taken from ref 41 (See Table 1 for bond distances). In all our calculations, the scalar relativistic second-order Douglas−Kroll−Hess (DKH) Hamiltonian[42−44] was used, together with relativistic semicore-contracted ANO-RCC-VTZP basis sets.[45]

Table 1. An−Cl Bond Lengths in Octahedral $[AnCl_6]^{3-}$ (from ref 5) and An−O Bond Lengths in Linear $[AnO_2]^{2+}$ (from ref 41) Used in the Calculations[a]

An	R(An−Cl)	R(An−O)
U	2.824	1.710
Np	2.799	1.700
Pu	2.777	1.675
Am	2.757	1.679

[a]All values are given in Å.

State average CASSCF calculations were performed for all species. For U(III), Np(III), Pu(III), and Am(III), the active space was CAS(n,7), where n = 3, 4, 5, and 6 electrons respectively in 7 orbitals. All possible configuration state functions (CSFs) generated from 5f-5f excitations within the above active spaces were included in the state average CASSCF calculations for U(III), Np(III), and Pu(III). For Am(III), the chosen active space generates 7 septets, 140 quintets, 588 triplets, and 490 singlets. To reduce the computational cost, we restricted ourselves to only 7 septets, 105 quintets, 378 triplets, and 323 singlets (based on an energy gap of ∼0.5−1 eV compared to the remaining states) (see Table S1).

For the trivalent hexachloride $[AnCl_6]^{3-}$ anions, the active space, state symmetry, and state average number of roots were the same as for the trivalent ions. The experimental optical spectra for $[AmCl_6]^{3-}$ were measured from the ionic salts.[46]

For the $[AnO_2]^{2+}$ cations, calculations were performed by using two different active spaces. One with 16 active orbitals (AS-I) and the other with 10 orbitals (AS-II). AS-I includes six bonding orbitals, mainly composed of the O 2p orbitals, seven An 5f orbitals, and three An 6d orbitals (Supporting Information). In the AS-II active space, the three strongly bonding and antibonding orbitals of "*gerade*" symmetry were removed compared to AS-I because their occupancies were close to 2 and 0 in all states, respectively, resulting in a 10-orbital active space (see Section 3.3 for more information). The number of roots, state symmetry, and active space details for the dioxides are summarized in Table S2.

For the multiconfigurational pair-density functional theory (MC-PDFT) calculations, the electron densities are taken from the corresponding multireference SA-CASSCF wave function and the total electronic energy is computed by using the nonclassical kinetic energy, classical Coulomb and nuclear-electron attraction energy, and an on-top electronic density functional (see eq 1). We used the translated "on-top" PBE functional (denoted as "tPBE") to compute the MC-PDFT energies.[15]

$$E_K^{\text{MC-PDFT}} = V_{\text{NN}} + \sum_{pq} D_{pq}^{KK} h_{pq} + \frac{1}{2}\sum_{pqrs} D_{pq}^{KK} D_{rs}^{KK} g_{pqrs} + E_{\text{ot}}(\rho_K, \Pi_K) \quad (1)$$

Here, V_{NN} is the nuclear repulsion energy, p, q, r, and s are generic orbital indices, D_{pq}^{KK} is the spinless reduced 1-particle density matrix for state K, h_{pq} is the one-electron matrix element including kinetic energy and electron−nuclear attraction, g_{pqrs} is a two-electron Coulomb matrix element, and E_{ot} is the on-top energy functional of the density ρ_{K} and on-top pair-density Π_{K}. We also performed hybrid MC-PDFT (HMC-PDFT) calculations, using the tPBE0 functional, in which λ = 0.25.[47] The energy expression for HMC-PDFT is

$$E_{\text{HMC-PDFT}} = \lambda E_{\text{MCWF}} + (1-\lambda)E_{\text{MC-PDFT}} \quad (2)$$

where E_{MCWF} is the CASSCF energy.

In the CMS-PDFT method, one chooses the intermediate state by maximizing the classical electron−electron repulsion (Coulomb) energy and the final CMS state energy is obtained by diagonalizing the effective Hamiltonian.[27]

Additionally, we performed state-specific CASPT2 (SS-CASPT2)[48] and extended multistate CASPT2[49] (XMS-CASPT2). Supersymmetry keywords such as "ATOM" for atoms and "LINEAR" for linear molecules were used to disable selected orbital rotations.

For the spin−orbit coupling, the RASSI-SO method was employed including all the spin−orbit free (SOF) states.[50] The atomic mean field integrals (AMFI) in the *Gateway* module were used to compute the spin−orbit integrals of each paramagnetic center.[51] An ultrafine grid was chosen in the *Seward* module for one- and two-electron integral calculations.

Notice that a formulation of MC-PDFT with the relativistic exact-two-component Hamiltonian (X2C-MC-PDFT) was presented,[34] but we do not use it here because it is not available for multistate versions of PDFT.

3. RESULTS AND DISCUSSION

3.1. An(III) Ions. We investigated four ions, namely, U(III), Np(III), Pu(III), and Am(III) for which accurate reference data are available. The total number of CSFs or spin−orbit free (SOF) states in D_{2h} symmetry for all four ions within CAS(n,7) is reported in Table S1. The ground-state J value

https://doi.org/10.1021/acs.jpca.3c05803
J. Phys. Chem. A 2023, 127, 9389−9397

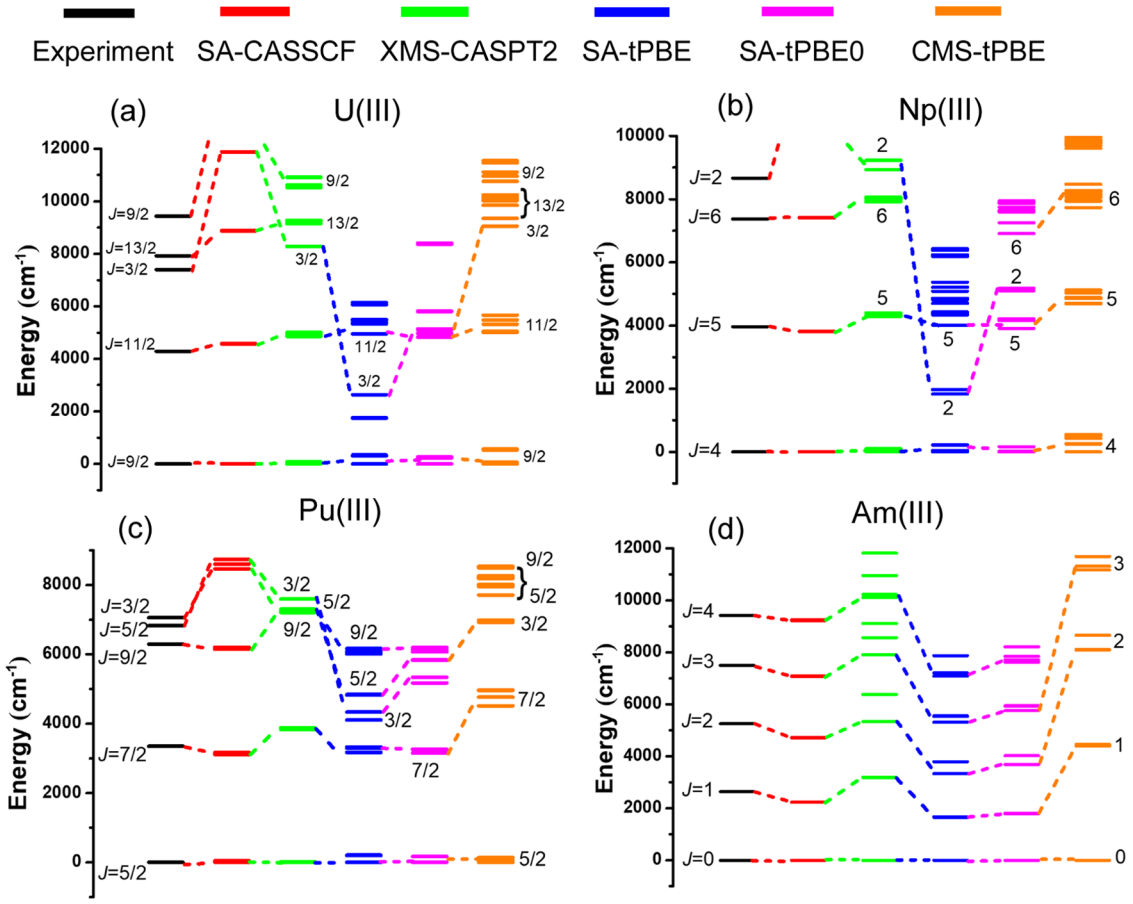

Figure 1. SO vertical excitation energies of free An(III) ions computed using various multireference methods along with the experimental values from ref 52. States within 9000−12 000 cm^{-1} above the respective ground states are plotted.

(spin−orbit coupled quantum number obtained from L−S coupling) for U(III) can be constructed from the coupling of S = 3/2 and L = 6 (I term) configuration (major contribution), which gives rise to the $^4I_{9/2}$ ground-state term (see Tables S3−S7). The ground-state term symbols for Np(III), Pu(III), and Am(III) are $^5I_4$, $^6H_{5/2}$, and $^7F_0$, respectively. Low-lying SO excited states within a window of 10000−12000 cm^{-1} from the ground state computed using SA-CASSCF, XMS-CASPT2, SA-tPBE, SA-tPBE0, and CMS-tPBE are shown in Figure 1 (see also Tables S3−S7 for the wave function decomposition). For the complete SO energy states and the wave function decomposition with respect to the S and L quantum numbers, see Tables S3−S26. Experimental excitation energy values were taken from ref 52.

Figure 1 shows that XMS-CASPT2 agrees the closest to the experimental data and reproduces the correct J ordering in all cases. For U(III), SA-CASSCF not only overestimates the J splitting but also predicts an incorrect J ordering due to the crossing between the 13/2 and 3/2 states. On the other hand, SA-tPBE and SA-tPBE0 underestimate the J splitting. Furthermore, SA-tPBE stabilizes lower J states more than other methods. Hybrid SA-tPBE0 improves the SO energies; however, the qualitative J ordering is still incorrect in some cases. A similar situation occurs for Np(III) and Pu(III). The CMS-tPBE relative energies are qualitatively more accurate than the SA-tPBE and SA-tPBE0 ones. However, there is a larger mixing of L and J-values in CMS-tPBE, which makes it difficult to assign the J and L quantum numbers (see Tables S27−S30).

Inspection of the major contributions arising from different L and S states shows that SA-tPBE and SA-tPBE0 stabilize lower L states more compared to SA-CASSCF and XMS-CASPT2, thus stabilizing the lower J states. Noticeably, the CMS-tPBE SOF relative energies are neither close to the XMS-CASPT2 nor the SA-CASSCF energies, suggesting that the improvement of CMS-tPBE occurs only at the SOC level (Tables S27−S30).

In the case of Am(III), the relative ordering of the J manifolds is the same for all of the methods (see Figure 1d). This is because the first four excited J levels arise due to the coupling of the L = 3 and S = 3 states, and there is scarcely any mixing between the higher-lying L (or S) states (see Table S25). While SA-tPBE and SA-tPBE0 underestimate the J splitting, CMS-tPBE-SO overestimates it compared with the experiment. The SA-CASSCF results agree better with the experiment compared with the other methods. Incorporating the lower-spin states, i.e., S = 2, 1, and 0 in the state average orbital optimization deteriorates the XMS-CASPT2 and CMS-tPBE results, while it improves the SA-CASSCF results. To assert this fact, we plotted the CMS-tPBE SO energies for three different cases: first, including all septets/quintets/triplets/singlets; second, including all septets/quintets/triplets; and third, including only septets and quintets (see Figure S1). We found that the CMS-tPBE-SO results for the third case match quite well with the experiment.

3.2. $[AnCl_6]^{3-}$ Anions. For the trivalent hexachloride anions, the SO energy-state ordering and wave function are similar to those of the free ions (see Figure 2 and Tables S31−

https://doi.org/10.1021/acs.jpca.3c05803
J. Phys. Chem. A 2023, 127, 9389−9397

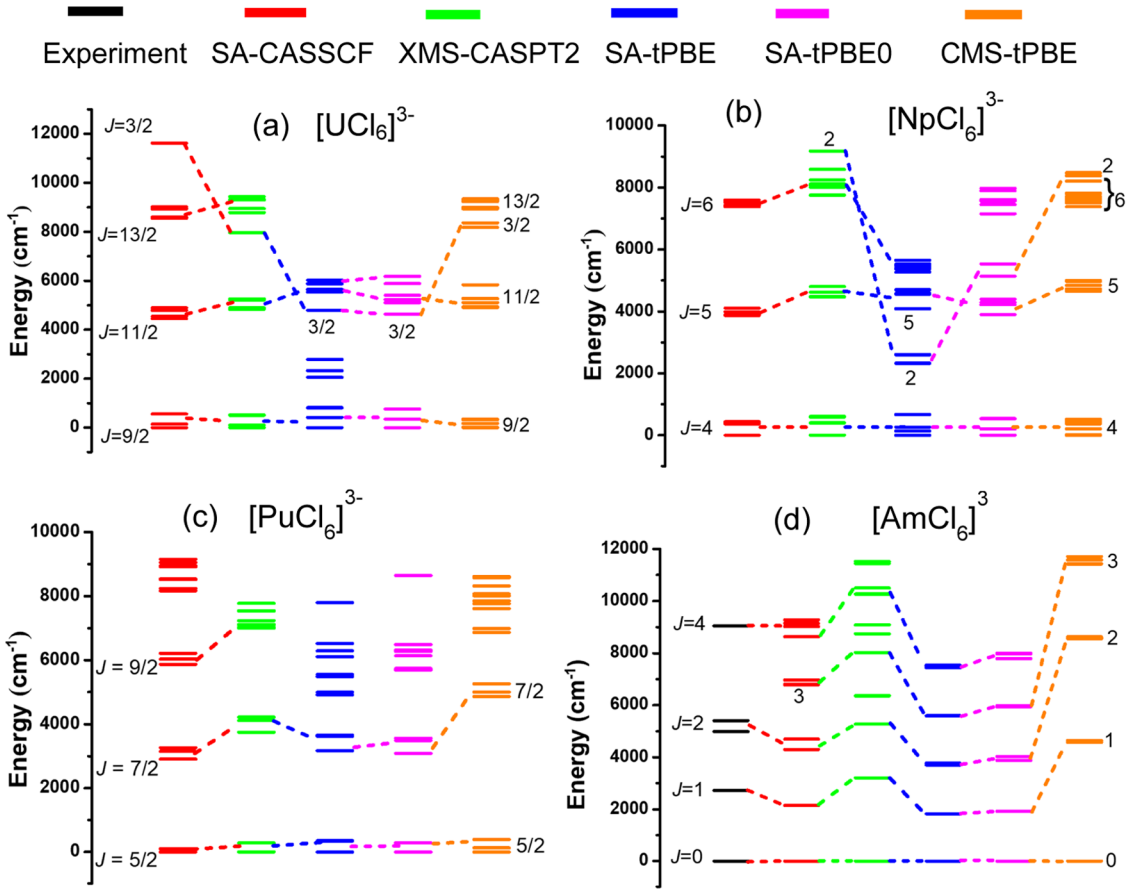

Figure 2. SO vertical excitation energies of $[An^{III}Cl_6]^{3-}$ anions computed using various multireference methods. For $[AmCl_6]^{3-}$ the experimental values have been taken from ref 46. States within 12 000 cm^{-1} from the ground state are plotted.

S34). In the case of molecules, the J quantum number is approximated as the ligand field mixes the eigenstates by lifting the degeneracy within the J level (i.e., m_J levels show a splitting); therefore, the J assignments have been made in analogy to the free ions and are based on the energies of the multiplets. Moreover, for excited states above 8000 cm^{-1}, the assignment of J becomes more difficult as the energy separation becomes small. Hence, some states are grouped together and labeled accordingly. The energies of the J = 13/2 and 3/2 states of $[UCl_6]^{3-}$ computed with CMS-tPBE are similar to those computed with XMS-CASPT2, and the same is true for the energies of the J = 6 and 2 states of $[NpCl_6]^{3-}$. Similar to the Am(III) free ion, the $[AmCl_6]^{3-}$ relative energies computed with XMS-CASPT2 and CMS-tPBE are highly overestimated compared with the experiment and other methods. As observed previously, the exclusion of higher-lying triplets and singlets from the SOF step yields a notable improvement in the energies, resulting in a closer alignment with the experiment J splitting (see Figure S1).

3.3. $[An^{VI}O_2]^{2+}$. Several CAS-based calculations on hexavalent dioxide cations have been reported. Gagliardi and Roos[53] studied the $[UO_2]^{2+}$ and other triatomic uranium molecules with CAS(12,12) active space. Later, Pierloot et al.[54] used CAS(12,16) and CAS(12,12) to compute the excited states for $[UO_2]^{2+}$, Réal et al.[55] used CAS(12,14) for the same molecule, and Infante et al.[41] performed CASPT2 calculations using both 14 orbital and 16 active orbitals to compute adiabatic energy gaps and ionization energies for various AnO_2, AnO_2^{+}, and AnO_2^{2+} species. These active spaces mostly consist of all the bonding 2p MOs on oxygen and different numbers of 5f and 6d orbitals on the actinide ion. Later, Gendron et al.[56,57] and Majumder et al.[58] have also used CAS(7,10) and CAS(8,10) for $[NpO_2]^{2+}$ and $[PuO_2]^{2+}$, respectively, to obtain vertical excitation energies. For $[AmO_2]^{2+}$, SO-CASPT2 calculations have been performed to obtain the excited states using an active space of CAS(15,13) by Notter et al.[59] We have used two different active spaces: (i) CAS(n, 16) (referred to as AS-I) and (ii) CAS(m, 10) (referred to as AS-II) throughout our calculations. Here, AS-I contains six bonding orbitals, σ_g, σ_u, two π_u, two π_g from the two oxygen atoms, seven U 5f orbitals of "*ungerade*" symmetry, and three virtual U 6d- σ_g and two π_g orbitals (see Figure S2). AS-II includes only the "*ungerade*" symmetric orbitals from the above 16-orbital sets and thus contains only 10 active orbitals (see Figure 3). In short, in the current work, we have used CAS (n, 16) in AS-I and CAS (m, 10) in AS-II, where n = 12, 13, 14, 15 and m = 6, 7, 8, 9 electrons for $[UO_2]^{2+}$, $[NpO_2]^{2+}$, $[PuO_2]^{2+}$, and $[AmO_2]^{2+}$, respectively (see Table S2). The geometries of the AnO_2^{2+} cations have been taken from the SO-CASPT2 calculations by Infante et al.[41] For an extensive spectroscopic analysis and thorough discussion regarding the electronic structures of the actinide oxides, we refer to the review by Kovács et al.[60] and other literature reports.[41,59,61−65]

To denote the SOF and SO states for the linear $[AnO_2]^{2+}$ species, we follow the standard molecular term symbol notation as $^{2S+1}\Lambda_{\Omega(g/u)}$, where the 2$S$+1 is the spin multiplicity, Λ denotes the projection of the total angular momentum along the internuclear axis, Ω is the projection of the total angular

https://doi.org/10.1021/acs.jpca.3c05803
J. Phys. Chem. A 2023, 127, 9389−9397

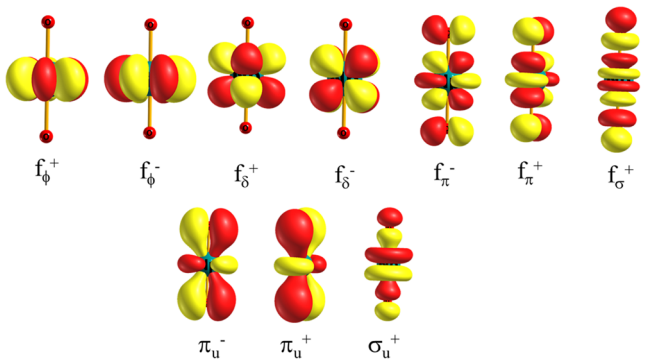

Figure 3. Example of natural orbitals from CAS(m,10) active space (AS-II), where m is the varying number of electrons in 10 active orbitals for the various An(VI) ions in hexavalent $[AnO_2]^{2+}$. The +/− is the reflection symmetry along an arbitrary plane containing the internuclear axis.

momentum along the internuclear axis, g or u indicate the symmetry or parity with respect to inversion through the center of symmetry.

The low-lying SOF- and SO-state energies are reported in Figure 4 (using AS-II) (see AS-I results in Figure S3 and Tables S35−S55). For the uranyl cation, the first four SO-excited states are dominated by triplet excited states and lie more than 15 000 cm^{-1} above the ground state. Going from the (6,10) to the (12,16) active space, the CASPT2 and SA-tPBE0 SO energies are almost unaffected, while SA-CASSCF energies are consistently overestimated and SA-tPBE energies are consistently underestimated (see Tables S35−S39). Here, the reason may be the dominant dynamic electron correlation in the $[UO_2]^{2+}$ cation. In the case of CMS-tPBE, the Ω ordering is incorrect for CAS(12,16) for the first four excited states; however, the ordering improves when the active space is reduced to (6,10) and it becomes closer to the SA-CASSCF results without further improvement.

Therefore, in the case of uranyl, CMS-tPBE does not improve the results compared to SA-tPBE and SA-tPBE0.

For neptunyl, both active-space results exhibit similar energetics for the first three excited Kramers pairs (Tables S40−S44). Here, SS-CASPT2 and XMS-CASPT2 underestimate the Ω splitting compared to the other methods. In the low-lying excited states (below 12 000 cm^{-1}), the dominating contribution to the SO states arises from the doublet SOF states; therefore, it can be inferred that static correlation is more prominent than dynamic correlation. Except for the CMS-tPBE energetics with CAS(13,16), all other methods show similar Ω ordering with both AS-I and AS-II. In the case of CAS(13,16), CMS-tPBE shows an additional Ω = 7/2 doublet in the third excited state, which is absent in all other cases (see Table S44). Although there is no experimental data available on bare $[NpO_2]^{2+}$, experimental excitation energies are reported for the $Cs_2UO_2Cl_4$ and $CsUO_2(NO_3)_3$ compounds in water.[65−67] We include these values in Table 2. The computed SO excited states for neptunyl ions are quite higher compared to the experimental

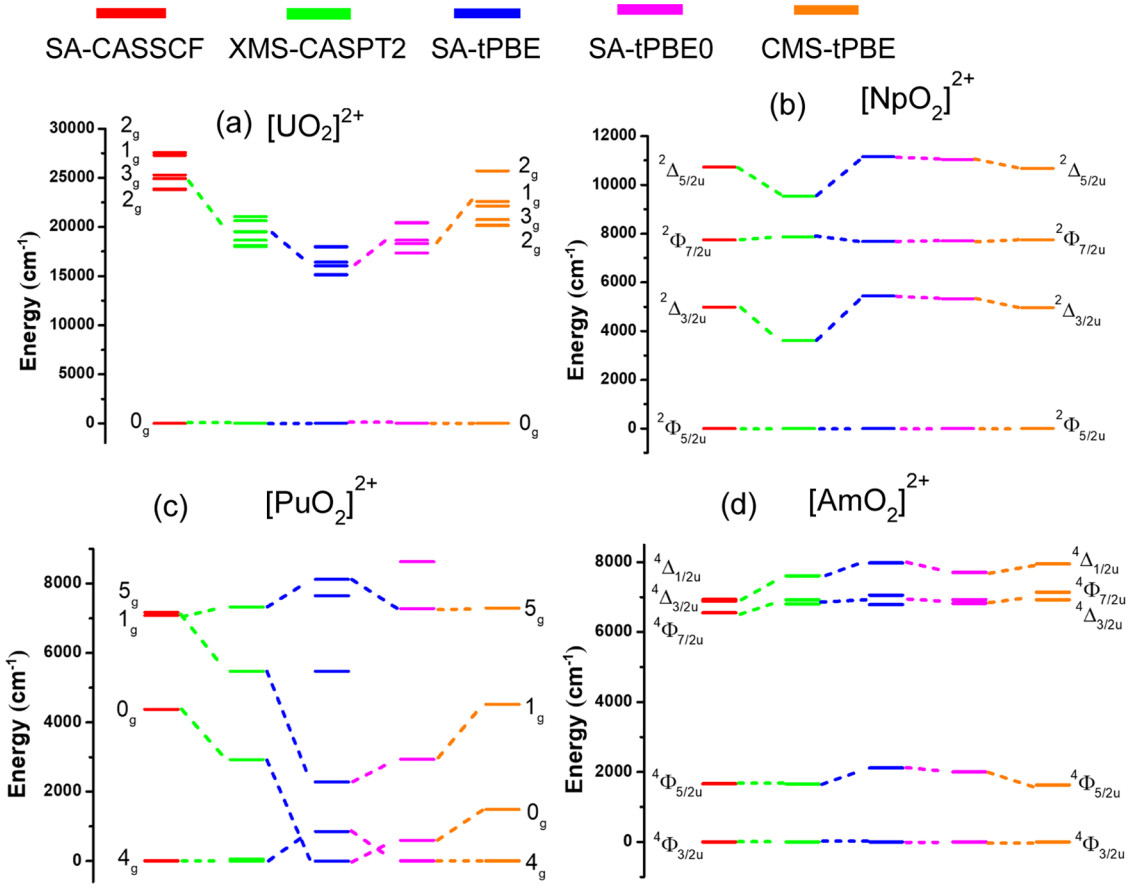

Figure 4. SO vertical excitation energies for hexavalent $[An^{VI}O_2]^{2+}$ cations were computed using various multireference methods with AS-II. Please check the text and Supporting Information for experimental values reported only for $[NpO_2]^{2+}$ and for $[PuO_2]^{2+}$.

https://doi.org/10.1021/acs.jpca.3c05803
J. Phys. Chem. A 2023, 127, 9389−9397

Table 2. Comparison of the Low-Lying Experimental SO Excitation Energies (in cm^{-1}) with the Computed Values Using the CAS(7,10) Active Space for the $[NpO_2]^{2+}$ Ion

Ω	$Cs_2NpO_2Cl_4$ (exp)	$CsNpO_2(NO_3)_3$ (exp)	SA-CASSCF	XMS-CASPT2	SA-tPBE	SA-tPBE0	CMS-tPBE
5/2u			0.0	0.0	0.0	0.0	0.0
3/2u	1000		4986	3615	5449	5332	4957
7/2u	6880	6459	7742	7869	7687	7702	7749
5/2u	7990	9420	10 732	9525	11 153	11 048	10 676

values, which may be attributed to the fact that the experimental values are obtained in water for a different species.

For plutonyl, both SA-tPBE and SA-tPBE0 energies for the low-lying SO states are lower compared to those of the other MR methods with both active spaces. Notably, SA-tPBE predicts the incorrect ground state with AS-II (i.e., CAS(8,10)) (see Figure 4c and Tables S45−S50). For this species, both CASPT2 and CMS-tPBE results are quite satisfactory with both active spaces and agree quite well with the experimental values (see Table S50).[65]

In the case of americyl, the AS-I results predict a different SO ground state with the SA-CASSCF and CASPT2 methods compared to the AS-II results (Figure S3 and Tables S51−S55). Although SA-tPBE, SA-tPBE0, and CMS-tPBE methods exhibit the correct SO ground state even with AS-I, the relative Ω splitting is underestimated by 2000−3000 cm^{-1} in the third and fourth excited states. On the other hand, the AS-II results are more consistent throughout all MR methods (see Figure 4d) even if the ordering of the $^4\Delta_{3/2u}$ and $^4\Phi_{7/2u}$ Kramers pairs is slightly different with each method. Our results with the CAS(9,10) active space are closer to the CAS(15,13) active space results in ref 59 on the same cation in terms of SO energies as well as Ω ordering. Hence, it is plausible that the utilization of only 32 state average roots might not adequately capture the SO excited-state energies with CAS(15,16). However, with this active space, it would not be computationally feasible to include more roots. An alternative approach would be to use restricted active space (RAS), employing the (15,16) active space with more than 32 roots, which may yield more precise and reliable outcomes.

4. SUMMARY AND CONCLUSIONS

In this study, we conducted a comprehensive analysis of the performance of PDFT methods in predicting the vertical excitation energies of various actinide systems. Our primary objective was to evaluate their accuracy in comparison to the established SA-CASSCF, XMS-CASPT2 approaches, and experimental data, thus establishing a benchmark for their efficacy in these systems.

Our findings reveal that in the context of trivalent free ions and hexachloride anions, the SA-tPBE methodology consistently exhibits a tendency to underestimate the J splitting, resulting in the stabilization of lower J-value states, which, with the other methods, are higher in energy. Notably, even with the application of SA-tPBE0, although enhancements in energy gap predictions are observed, the relative J ordering remains inaccurate. In contrast, the CMS-PDFT approach yields significant improvements in the accurate prediction of the J splitting. Furthermore, the resulting J ordering aligns notably well with the experiment and XMS-CASPT2, especially when considering energy levels below ∼8000 cm^{-1}.

Within the framework of CMS-PDFT, the diagonal components are extracted from MC-PDFT energies, while the off-diagonal elements incorporate CASSCF exchange effects within the intermediate basis. This integration of CASSCF exchange brings about a significant enhancement in the methodology. However, this improvement comes at a cost; it leads to a stronger mixing of the L quantum numbers, subsequently influencing the J quantum number. Consequently, the J values produced by CMS-PDFT exhibit notable deviations from the anticipated integer or half-integer values.

This phenomenon also applies to hexachloride anions. In these instances, the J ordering and assignment within CMS-PDFT exhibit a higher agreement with XMS-CASPT2-SO, especially for states lying up to 10 000 cm^{-1} above their respective ground states. Notably, this alignment between CMS-PDFT and XMS-CASPT2 improves the SO calculations compared to the SOF calculations.

For the actinyl species, our investigation encompassed two distinct active spaces, each yielding differing outcomes. Notably, in the context of vertical SO energies, the smaller active space (AS-II), comprising 10 orbitals, exhibits more favorable performance compared with the larger counterpart (AS-I), comprising 16 orbitals. The inferior performance of AS-I, particularly evident for $[PuO_2]^{2+}$ and $[AmO_2]^{2+}$, may be attributed to the insufficient number of states that could be employed in the calculations. To address this issue when dealing with large active spaces such as AS-I, a more effective approach could involve the integration of a RAS-based methodology, which can accommodate a larger number of states. Importantly, SA-tPBE0 and CMS-PDFT perform better when a smaller active space with more than 40 state average roots is chosen for every species. An example is the case of $[UO_2]^{2+}$, where SA-tPBE0 outperforms SA-CASSCF, SA-tPBE, and CMS-tPBE.

The key takeaway from this study resides in the substantial promise exhibited by PDFT methods in the context of actinide systems. This is underscored by the evident necessity for large active spaces in these systems coupled with the comparatively reduced computational expense of PDFT calculations relative to their CASPT2 counterparts.

Among the PDFT methodologies explored, CMS-PDFT emerges as the standout performer due to its inherent multistate nature. As such, the continued advancement of multistate PDFT[68] methods holds pivotal importance in effectively addressing the intricacies of actinide systems.

■ ASSOCIATED CONTENT

Supporting Information

The Supporting Information is available free of charge at https://pubs.acs.org/doi/10.1021/acs.jpca.3c05803.

Active-space description; relative electronic energies computed with different methods; wave function decomposition (PDF)

https://doi.org/10.1021/acs.jpca.3c05803
J. Phys. Chem. A 2023, 127, 9389−9397

AUTHOR INFORMATION

Corresponding Author

Laura Gagliardi − *Department of Chemistry, Pritzker School of Molecular Engineering, James Franck Institute, Director of the Chicago Center for Theoretical Chemistry, The University of Chicago, Chicago, Illinois 60637, United States; Argonne National Laboratory, Lemont, Illinois 60439, United States;* orcid.org/0000-0001-5227-1396; Email: lgagliardi@uchicago.edu

Author

Arup Sarkar − *Department of Chemistry, The University of Chicago, Chicago, Illinois 60637, United States;* orcid.org/0000-0002-6880-8220

Complete contact information is available at: https://pubs.acs.org/10.1021/acs.jpca.3c05803

Author Contributions

The manuscript was written through contributions of both authors. Both authors have given approval to the final version of the manuscript

Funding

This work was funded by the Division of Chemical Sciences, Geosciences, and Biosciences, Office of Basic Energy Sciences, U.S. Department of Energy, through Grant DE-SC0022572.

Notes

The authors declare no competing financial interest.

ACKNOWLEDGMENTS

The authors are thankful to Jie J. Bao and Donald G. Truhlar, University of Minnesota, and Matthew R. Hermes, University of Chicago, for useful discussions and suggestions for this work. The authors acknowledge the University of Chicago Research Computing Center (RCC) for providing computational resources.

REFERENCES

(1) Ewing, R. C. Nuclear Waste Forms for Actinides. *Proc. Natl. Acad. Sci. U.S.A.* **1999**, *96* (7), 3432−3439.

(2) Veliscek-Carolan, J. Separation of Actinides from Spent Nuclear Fuel: A Review. *J. Hazard. Mater.* **2016**, *318*, 266−281.

(3) King, D. M.; Cleaves, P. A.; Wooles, A. J.; Gardner, B. M.; Chilton, N. F.; Tuna, F.; Lewis, W.; McInnes, E. J. L.; Liddle, S. T. Molecular and Electronic Structure of Terminal and Alkali Metal-Capped Uranium(V) Nitride Complexes. *Nat. Commun.* **2016**, *7* (1), No. 13773.

(4) Rinehart, J. D.; Long, J. R. Slow Magnetic Relaxation in Homoleptic Trispyrazolylborate Complexes of Neodymium(iii) and Uranium(iii). *Dalton Trans.* **2012**, *41* (44), 13572−13574.

(5) Jung, J.; Atanasov, M.; Neese, F. Ab Initio Ligand-Field Theory Analysis and Covalency Trends in Actinide and Lanthanide Free Ions and Octahedral Complexes. *Inorg. Chem.* **2017**, *56* (15), 8802−8816.

(6) Meihaus, K. R.; Long, J. R. Actinide-Based Single-Molecule Magnets. *Dalton Trans.* **2015**, *44* (6), 2517−2528.

(7) Ray, D.; Oakley, M. S.; Sarkar, A.; Bai, X.; Gagliardi, L. Theoretical Investigation of Single-Molecule-Magnet Behavior in Mononuclear Dysprosium and Californium Complexes. *Inorg. Chem.* **2023**, *62* (4), 1649−1658.

(8) Küchle, W.; Dolg, M.; Stoll, H. Ab Initio Study of the Lanthanide and Actinide Contraction. *J. Phys. Chem. A* **1997**, *101* (38), 7128−7133.

(9) Gagliardi, L.; Roos, B. O. Multiconfigurational Quantum Chemical Methods for Molecular Systems Containing Actinides. *Chem. Soc. Rev.* **2007**, *36* (6), 893−903.

(10) Ciborowski, S. M.; Mitra, A.; Harris, R. M.; Liu, G.; Sharma, P.; Khetrapal, N.; Blankenhorn, M.; Gagliardi, L.; Bowen, K. H. Metal-Metal Bonding in Actinide Dimers: U_2 and U^{2-}. *J. Am. Chem. Soc.* **2021**, *143* (41), 17023−17028.

(11) Singh, S. K.; Cramer, C. J.; Gagliardi, L. Correlating Electronic Structure and Magnetic Anisotropy in Actinide Complexes [An-$(COT)_2$], AnIII/IV = U, Np, and Pu. *Inorg. Chem.* **2020**, *59* (10), 6815−6825.

(12) Yu, X.; Sergentu, D. C.; Feng, R.; Autschbach, J. Covalency of Trivalent Actinide Ions with Different Donor Ligands: Do Density Functional and Multiconfigurational Wavefunction Calculations Corroborate the Observed "Breaks"? *Inorg. Chem.* **2021**, *60* (23), 17744−17757.

(13) Gagliardi, L.; Roos, B. O. Quantum Chemical Calculations Show That the Uranium Molecule U_2 Has a Quintuple Bond. *Nature* **2005**, *433* (7028), 848−851.

(14) Gaggioli, C. A.; Gagliardi, L. Theoretical Investigation of Plutonium-Based Single-Molecule Magnets. *Inorg. Chem.* **2018**, *57* (14), 8098−8105.

(15) Li Manni, G.; Carlson, R. K.; Luo, S.; Ma, D.; Olsen, J.; Truhlar, D. G.; Gagliardi, L. Multiconfiguration Pair-Density Functional Theory. *J. Chem. Theory Comput.* **2014**, *10* (9), 3669−3680.

(16) Gagliardi, L.; Truhlar, D. G.; Manni, G. L.; Carlson, R. K.; Hoyer, C. E.; Bao, J. L. Multiconfiguration Pair-Density Functional Theory: A New Way to Treat Strongly Correlated Systems. *Acc. Chem. Res.* **2017**, *50* (1), 66−73.

(17) Stroscio, G. D.; Zhou, C.; Truhlar, D. G.; Gagliardi, L. Multiconfiguration Pair-Density Functional Theory Calculations of Iron(II) Porphyrin: Effects of Hybrid Pair-Density Functionals and Expanded RAS and DMRG Active Spaces on Spin-State Orderings. *J. Phys. Chem. A* **2022**, *126* (24), 3957−3963.

(18) Ghosh, S.; Cramer, C. J.; Truhlar, D. G.; Gagliardi, L. Generalized-Active-Space Pair-Density Functional Theory: An Efficient Method to Study Large, Strongly Correlated, Conjugated Systems. *Chem. Sci.* **2017**, *8* (4), 2741−2750.

(19) Pandharkar, R.; Hermes, M. R.; Cramer, C. J.; Truhlar, D. G.; Gagliardi, L. Localized Active Space Pair-Density Functional Theory. *J. Chem. Theory Comput.* **2021**, *17* (5), 2843−2851.

(20) Sharma, P.; Bernales, V.; Knecht, S.; Truhlar, D. G.; Gagliardi, L. Density Matrix Renormalization Group Pair-Density Functional Theory (DMRG-PDFT): Singlet-Triplet Gaps in Polyacenes and Polyacetylenes. *Chem. Sci.* **2019**, *10* (6), 1716−1723.

(21) Sharma, P.; Truhlar, D. G.; Gagliardi, L. Magnetic Coupling in a Tris-Hydroxo-Bridged Chromium Dimer Occurs through Ligand Mediated Superexchange in Conjunction with Through-Space Coupling. *J. Am. Chem. Soc.* **2020**, *142* (39), 16644−16650.

(22) Zhou, C.; Hermes, M. R.; Wu, D.; Bao, J. J.; Pandharkar, R.; King, D. S.; Zhang, D.; Scott, T. R.; Lykhin, A. O.; Gagliardi, L.; Truhlar, D. G. Electronic Structure of Strongly Correlated Systems: Recent Developments in Multiconfiguration Pair-Density Functional Theory and Multiconfiguration Nonclassical-Energy Functional Theory. *Chem. Sci.* **2022**, *13* (26), 7685−7706.

(23) Adeyiga, O.; Suleiman, O.; Dandu, N. K.; Odoh, S. O. Ground-State Actinide Chemistry with Scalar-Relativistic Multiconfiguration Pair-Density Functional Theory. *J. Chem. Phys.* **2019**, *151* (13), No. 134102.

(24) Hu, S. X.; You, X. X.; Zou, W. L.; Lu, E.; Gao, X.; Zhang, P. Electronic Structures and Unusual Chemical Bonding in Actinyl Peroxide Dimers $[An_2O_6]^{2+}$ and $[(An_2O_6)(12\text{-Crown-4 Ether})_2]^{2+}$ (An = U, Np, and Pu). *Inorg. Chem.* **2022**, *61* (39), 15589−15599.

(25) Finley, J.; Malmqvist, P.-Å.; Roos, B. O.; Serrano-Andrés, L. The Multi-State CASPT2 Method. *Chem. Phys. Lett.* **1998**, *288* (2), 299−306.

(26) Angeli, C.; Borini, S.; Cestari, M.; Cimiraglia, R. A Quasidegenerate Formulation of the Second Order N-Electron Valence State Perturbation Theory Approach. *J. Chem. Phys.* **2004**, *121* (9), 4043−4049.

(27) Bao, J. J.; Zhou, C.; Truhlar, D. G. Compressed-State Multistate Pair-Density Functional Theory. *J. Chem. Theory Comput.* **2020**, *16* (12), 7444−7452.
(28) Bao, J. J.; Zhou, C.; Varga, Z.; Kanchanakungwankul, S.; Gagliardi, L.; Truhlar, D. G. Multi-State Pair-Density Functional Theory. *Faraday Discuss.* **2020**, *224* (0), 348−372.
(29) Bao, J. J.; Hermes, M. R.; Scott, T. R.; Sand, A. M.; Lindh, R.; Gagliardi, L.; Truhlar, D. G. Analytic Gradients for Compressed Multistate Pair-Density Functional Theory. *Mol. Phys.* **2022**, *120* (19−20), No. e2110534, DOI: 10.1080/00268976.2022.2110534.
(30) Lykhin, A. O.; Baumgarten, M. K. A.; Truhlar, D. G.; Gagliardi, L. Dipole Moments and Transition Dipole Moments Calculated by Pair-Density Functional Theory with State Interaction. *J. Phys. Chem. A* **2023**, *127* (18), 4194−4205.
(31) Knecht, S.; Jensen, H. J. A.; Saue, T. Relativistic Quantum Chemical Calculations Show That the Uranium Molecule U_2 Has a Quadruple Bond. *Nat. Chem.* **2019**, *11*, 40−44.
(32) Hu, H.; Jenkins, A. J.; Liu, H.; Kasper, J. M.; Frisch, M. J.; Li, X. Relativistic Two-Component Multireference Configuration Interaction Method with Tunable Correlation Space. *J. Chem. Theory Comput.* **2020**, *16* (5), 2975−2984.
(33) Lu, L.; Hu, H.; Jenkins, A. J.; Li, X. Exact-Two-Component Relativistic Multireference Second-Order Perturbation Theory. *J. Chem. Theory Comput.* **2022**, *18* (5), 2983−2992.
(34) Sharma, P.; Jenkins, A. J.; Scalmani, G.; Frisch, M. J.; Truhlar, D. G.; Gagliardi, L.; Li, X. Exact-Two-Component Multiconfiguration Pair-Density Functional Theory. *J. Chem. Theory Comput.* **2022**, *18* (5), 2947−2954.
(35) Wu, D.; Zhou, C.; Bao, J. J.; Gagliardi, L.; Truhlar, D. G. Zero-Field Splitting Calculations by Multiconfiguration Pair-Density Functional Theory. *J. Chem. Theory Comput.* **2022**, *18* (4), 2199−2207.
(36) Sauza-de la Vega, A.; Pandharkar, R.; Stroscio, G. D.; Sarkar, A.; Truhlar, D. G.; Gagliardi, L. Multiconfiguration Pair-Density Functional Theory for Chromium(IV) Molecular Qubits. *JACS Au* **2022**, *2* (9), 2029−2037.
(37) Goh, T.; Pandharkar, R.; Gagliardi, L. Multireference Study of Optically Addressable Vanadium-Based Molecular Qubit Candidates. *J. Phys. Chem. A* **2022**, *126* (36), 6329−6335.
(38) Layfield, R. A.; Murugesu, M. *Lanthanides and Actinides in Molecular Magnetism*; John Wiley & Sons, 2015.
(39) Liu, M.; Peng, X.; Guo, F.; Tong, M.-L. Actinide-Based Single-Molecule Magnets : Alone or in a Group ? *Inorg. Chem. Front.* **2023**, *10* (13), 3742−3755.
(40) Li Manni, G.; Galván, I. F.; Alavi, A.; Aleotti, F.; Aquilante, F.; Autschbach, J.; Avagliano, D.; Baiardi, A.; Bao, J. J.; Battaglia, S.; et al. The OpenMolcas Web: A Community-Driven Approach to Advancing Computational Chemistry. *J. Chem. Theory Comput.* **2023**, *19*, 6933−6991, DOI: 10.1021/acs.jctc.3c00182.
(41) Infante, I.; Kovacs, A.; MacChia, G. La.; Shahi, A. R. M.; Gibson, J. K.; Gagliardi, L. Ionization Energies for the Actinide Mono- and Dioxides Series, from Th to Cm: Theory versus Experiment. *J. Phys. Chem. A* **2010**, *114* (19), 6007−6015.
(42) Hess, B. A. Relativistic Electronic-Structure Calculations Employing a Two-Component No-Pair Formalism with External-Field Projection Operators. *Phys. Rev. A* **1986**, *33* (6), 3742−3748.
(43) Wolf, A.; Reiher, M. Exact Decoupling of the Dirac Hamiltonian. III. Molecular Properties. *J. Chem. Phys.* **2006**, *124* (6), 64102.
(44) Wolf, A.; Reiher, M. Exact Decoupling of the Dirac Hamiltonian. IV. Automated Evaluation of Molecular Properties within the Douglas-Kroll-Hess Theory up to Arbitrary Order. *J. Chem. Phys.* **2006**, *124* (6), 64103.
(45) Roos, B. O.; Lindh, R.; Malmqvist, P.-Å.; Veryazov, V.; Widmark, P.-O. New Relativistic ANO Basis Sets for Actinide Atoms. *Chem. Phys. Lett.* **2005**, *409* (4), 295−299.
(46) Barbanel', Y. A.; Chudnovskaya, G. P.; Dushin, R. B.; Kolin, V. V.; Kotlin, V. P.; Nekhoroshkov, S. N.; Pen'kin, M. V. Optical Spectra and Crystal Field of Am^{3+} and Cm^{3+} in the Cubic Elpasolite Crystals. *Radiochim. Acta* **1997**, *78* (s1), 69−72, DOI: 10.1524/ract.1997.78.-special-issue.69.
(47) Pandharkar, R.; Hermes, M. R.; Truhlar, D. G.; Gagliardi, L. A New Mixing of Nonlocal Exchange and Nonlocal Correlation with Multiconfiguration Pair-Density Functional Theory. *J. Phys. Chem. Lett.* **2020**, *11* (23), 10158−10163.
(48) Andersson, K.; Malmqvist, P. A.; Roos, B. O.; Sadlej, A. J.; Wolinski, K. Second-Order Perturbation Theory with a CASSCF Reference Function. *J. Phys. Chem. A* **1990**, *94* (14), 5483−5488.
(49) Shiozaki, T.; Győrffy, W.; Celani, P.; Werner, H.-J. Communication: Extended Multi-State Complete Active Space Second-Order Perturbation Theory: Energy and Nuclear Gradients. *J. Chem. Phys.* **2011**, *135* (8), 81106.
(50) Malmqvist, P. Å.; Roos, B. O.; Schimmelpfennig, B. The Restricted Active Space (RAS) State Interaction Approach with Spin−Orbit Coupling. *Chem. Phys. Lett.* **2002**, *357* (3), 230−240.
(51) Heß, B. A.; Marian, C. M.; Wahlgren, U.; Gropen, O. A Mean-Field Spin-Orbit Method Applicable to Correlated Wavefunctions. *Chem. Phys. Lett.* **1996**, *251* (5), 365−371.
(52) Carnall, W. T.; Wybourne, B. G. Electronic Energy Levels of the Lighter Actinides: U^{3+}, Np^{3+}, Pu^{3+}, Am^{3+}, and Cm^{3+}. *J. Chem. Phys.* **1964**, *40*, 3428−3433.
(53) Gagliardi, L.; Roos, B. O. Uranium Triatomic Compounds XUY (X,Y = C,N,O): A Combined Multiconfigurational Second-Order Perturbation and Density Functional Study. *Chem. Phys. Lett.* **2000**, *331* (2), 229−234.
(54) Pierloot, K.; Van Besien, E. Electronic Structure and Spectrum of $UO_2^{2+}$and $UO_2CI_4^{2-}$. *J. Chem. Phys.* **2005**, *123* (20), No. 204309.
(55) Réal, F.; Vallet, V.; Marian, C.; Wahlgren, U. Theoretical Investigation of the Energies and Geometries of Photoexcited Uranyl(VI) Ion: A Comparison between Wave-Function Theory and Density Functional Theory. *J. Chem. Phys.* **2007**, *127* (21), No. 214302.
(56) Gendron, F.; Pritchard, B.; Bolvin, H.; Autschbach, J. Magnetic Resonance Properties of Actinyl Carbonate Complexes and Plutonyl-(VI)-Tris-Nitrate. *Inorg. Chem.* **2014**, *53* (16), 8577−8592.
(57) Gendron, F.; Páez-Hernández, D.; Notter, F. P.; Pritchard, B.; Bolvin, H.; Autschbach, J. Magnetic Properties and Electronic Structure of Neptunyl(VI) Complexes: Wavefunctions, Orbitals, and Crystal-Field Models. *Chem. − Eur. J.* **2014**, *20* (26), 7994−8011.
(58) Majumder, R.; Sokolov, A. Y. Simulating Spin-Orbit Coupling with Quasidegenerate N-Electron Valence Perturbation Theory. *J. Phys. Chem. A* **2023**, *127* (2), 546−559.
(59) Notter, F. P.; Dubillard, S.; Bolvin, H. A Theoretical Study of the Excited States of AmO_2^{n+}, n = 1,2,3. *J. Chem. Phys.* **2008**, *128*, No. 164315.
(60) Kovács, A.; Konings, R. J. M.; Gibson, J. K.; Infante, I.; Gagliardi, L. Quantum Chemical Calculations and Experimental Investigations of Molecular Actinide Oxides. *Chem. Rev.* **2015**, *115* (4), 1725−1759.
(61) La Macchia, G.; Infante, I.; Raab, J.; Gibson, J. K.; Gagliardi, L. A Theoretical Study of the Ground State and Lowest Excited States of $PuO^{0/+/+2}$ and $PuO_2^{0/+/+2}$. *Phys. Chem. Chem. Phys.* **2008**, *10* (48), 7278−7283.
(62) Averkiev, B. B.; Mantina, M.; Valero, R.; Infante, I.; Kovacs, A.; Truhlar, D. G.; Gagliardi, L. How Accurate Are Electronic Structure Methods for Actinoid Chemistry? *Theor. Chem. Acc.* **2011**, *129* (3−5), 657−666.
(63) Réal, F.; Gomes, A. S. P.; Visscher, L.; Vallete, V.; Eliav, E. Benchmarking Electronic Structure Calculations on the Bare UO_2^{2+} Ion: How Different Are Single and Multireference Electron Correlation Methods? *J. Phys. Chem. A* **2009**, *113* (45), 12504−12511.
(64) Hay, P. J.; Martin, R. L.; Schreckenbach, G. Theoretical Studies of the Properties and Solution Chemistry of AnO_2^{2+} and AnO^{2+} Aquo Complexes for An = U, Np, and Pu. *J. Phys. Chem. A* **2000**, *104* (26), 6259−6270.
(65) Infante, I.; Gomes, A. S. P.; Visscher, L. On the Performance of the Intermediate Hamiltonian Fock-Space Coupled-Cluster Method

on Linear Triatomic Molecules: The Electronic Spectra of NpO_2^+, NpO_2^{2+}, and PuO_2^{2+}. *J. Chem. Phys.* **2006**, *125*, No. 074301.
(66) Denning, R. G.; Norris, J. O. W.; Brown, D. The Electronic Structure of Actinyl Ions. *Mol. Phys.* **1982**, *46* (2), 287−323.
(67) Matsika, S.; Pitzer, R. M. Electronic Spectrum of the NpO_2^{2+} and NpO_2^+ Ions. *J. Phys. Chem. A* **2000**, *104* (17), 4064−4068.
(68) Hennefarth, M. R.; Hermes, M. R.; Truhlar, D. G.; Gagliardi, L. Linearized Pair-Density Functional Theory. *J. Chem. Theory Comput.* **2023**, *19* (11), 3172−3183.

https://doi.org/10.1021/acs.jpca.3c05803
J. Phys. Chem. A 2023, 127, 9389−9397